## Scientific-Research Article

# Mixed Mode (I/II/III) Stress Intensity Factors in Gas Turbine Blade Considering 3D Semi-Elliptical Crack

Seyed mohammad navid Ghoreishi[1]* , Nabi Mehri-Khansari [2] , Houman Rezaei[3]

1-Satellite Research Institute, Iranian Space Research Center, Tehran, Iran
2-Faculty of Mechanical Engineering, Sahand University of Technology, Tabriz, Iran
3-Departments of Mechanics and Systems, University of Polytechnic of Tours, France

## ABSTRACT

*Regardless of the initiation or propagation procedure of crack in a gas turbine blade, the precise expectation of the fracture behavior, such as mixed-mode Stress Intensity Factors (SIF), plays a significant role in acquiring its operational life. Therefore, multilateral three-dimensional fracture solutions are required, including real-based mixed-mode loading (I/II/III) conditions and geometrical considerations. In this study, three-dimensional semi-elliptical crack in a gas turbine blade with various geometrical parameters and inclination angles under mixed-mode loading (I/II/III) conditions were investigated based on the employed finite element techniques and analytical procedure. In this context, the semi-elliptical crack has been considered in the critical zone of the rotating blade to achieve the effect of crack aspect ratio, rotational velocity, crack location, and mechanical properties. Fluid Solid Interaction (FSI) analysis was also performed in addition to solid functional enriched elements. Structural simulation has been conducted at the speed of 83.776 m/s based on CFD simulation. The results indicated that Al Alloys blade shows a profitable resistance in crack propagation. Moreover, as the crack domain is near the location of x/c= 0.25 and 1.9 of crack front, the mode II SIF will be independent of rotational velocity and the blades' mechanical properties. Similarly, for the location of x/c= 1.1 in crack front, the mode III SIF is independent of rotational velocity and blades' mechanical properties.*

## Introduction

Consider the widespread attention of gas turbines in various industries such as aerospace and petroleum; consideration of the failure analysis became one of the main concerns in the design and maintenance of these structures. Most failures are due to rotating components (Tao, Zhong, & Li, 2000), in which rotor blades account for about half of the failure in the rotating components (Montoya, 1966). Failure not only changes the gas path lines but can also cause the degradation of the stage and reduction of efficiencies. Therefore, the health monitoring conditions of blades in gas turbines are the most

significant part of fault detection process. In this context, efficient methods for estimating the turbine performance and the error detection have been proposed (Boyce, 2011; Lakshminarasimha, Boyce, & Meher-Homji, 1994; Li, 2010). Also, fault diagnoses were analyzed by combining different finite elements and fractographic analysis (Farrahi, Tirehdast, Abad, Parsa, & Motakefpoor, 2011). In 2016, Ying et al. (Ying, Cao, Li, Li, & Guo, 2016) proposed a fault detection technique of gas-path by developing robustness using a theoretical approach. Performance degradation was identified based on actual operational data and neural networks (Li, 2010). Although the grading model is very practical, it has limitations, such as a unique focus on the degradation performance.

Because geometrical status can have a significant role in fault detection and degradation performance, Dengji et al. (Zhou, Wei, Huang, Li, & Zhang, 2020) changed the blade profile and geometrical conditions of crack to obtain fault diagnosis numerically. Several types of research investigated the compressor efficiency by variation of geometrical parameters of the blade, such as the leading-edge thickness (e.g. (Kumar, Keane, Nair, & Shahpar, 2006), (Sarraf, Nouri, Ravelet, & Bakir, 2011)). Different types of cracks in turbine blade and the evolution of crack propagation should be considered. It was ascertained that simple straight edge/ through crack could not completely represent the crack propagation, whereas semi-elliptical cracks can address the real behavior of crack propagation because Lin and Smith (Lin & Smith, 1998a) proved that any surface crack after partial propagation becomes a semi-elliptical crack. Therefore, semi-elliptical cracks can simulate the actual behavior of cracks in different structures.

Amara Mouna et al. (Mouna et al., 2019) applied a numerical approach to predict crack paths using semi-elliptical crack modeling. Moreover, theoretical and experimental considerations ascertained that airflow and rotational speed of the turbine induced a fatigue failure of cyclic loading. Generally, NDT methods, including virtual inspection, fractography in addition to numerical and analytical methods, have been proposed to analyze the failure of gas turbine blades under fatigue loading (Hirakawa, Toyama, & Kubota, 1998; Nowell, Dini, & Hills, 2006; Xi, Zhong, Huang, Yan, & Tao, 2000). Therefore, several scholars have been reported to investigate fatigue failure (Hou, Wicks, & Antoniou, 2002; Kumari,

Satyanarayana, & Srinivas, 2014; Yingyu Wang & Susmel, 2016; Yu, Zhu, Liu, & Liu, 2017) and creep (Ghatak & Robi, 2016; Poursaeidi, Aieneravaie, & Mohammadi, 2008) in the first and the second gas turbine blades. Velásquez et al. (Viswanathan & Dolbec, 1987) and Guo et al. (Guo et al., 2019) considered degradation and the maximum service conditions of the turbine blade to account for both creep and fatigue. Suder et al. (Suder, Chima, Strazisar, & Roberts, 1995) and Garzon et al. (Garzon & Darmofal, 2003) investigated the effect of impact parameters on the compressor efficiency and the pressure ratio using multistage compressor model experimentally. Since numerical methods can simulate failure analysis, several considerations have been proposed. For instance, the numerical approach has been studied for failure prediction and life assessment of the first and the second blade consideration of dynamic characteristics and harmonic analyses of 2D. (Kersey, Staroselsky, Dudzinski, & Genest, 2013; Poursaeidi et al., 2008) and 3D FEM Chen and Xie (L.-j. Chen & Xie, 2005) presented a finite element model for predicting the low cycle fatigue life using aerodynamic coupling and low-pressure turbine blades.

Experiment procedure of testing set up for a gas turbine blade failure is very expensive, so the numerical methods have been employed (Kirthan, Hegde, Suresh, & Kumar, 2014; Poursaeidi & Salavatian, 2009; L. J. E. F. A. Witek, 2015; L. J. F. o. A. S. Witek, 2012). Kumar et al. (Kumar, Nair, Keane, & Shahpar, 2005) presented a numerical approach including uncertainty for detecting the corrosion in blade performance. Funazaki et al. (Funazaki et al., 2001) applied a numerical model and experimental procedure to evaluate the heat transfer in the turbine blade. Yasmina et al. (Yasmina, Bacha, & Semmar, 2008) proposed a numerical-based probability model (Monte Carlo method) to simulate the erosion and fatigue failure for turbine blades. Moreover, Computational Fluid Dynamics (CFD) simulations and experimental investigations are common methods to study the mechanism of performance. In this context, Lange et al. (Lange, Vogeler, Schrapp, & Clemen, 2009) proposed 3D optical techniques to represent the geometrical parameters of the blade, such as the chord length and to apply the Monte Carlo method to study the blade manufacturing misalignment encountering to the aerodynamic loading. Yang et al. (Yang, Hui, & Guo-tai, 2011) proposed a numerical simulation based on the fluid thermal

model and the geometrical accuracy validated by an experimental test. Morini et al. (Morini, Pinelli, Spina, & Venturini, 2011) evaluated the effect of fouling blades roughness on the blade performance. Shojaeifard et al. (Shojaeifard, Sajedin, & Khalkhali, 2019) proposed a numerical study based on fluid-solid interaction in which the effect of blade geometrical variation was considered on compressor's performance.

Thermal fatigue can lead to emerging macrocracks and service life, especially for some superalloys such as Ni-based superalloys (Kersey et al., 2013). Also, various cracks configurations can be induced in gas turbine blades due to the pre-twisting and cooling stage (Liu, Yang, Li, & Shi, 2020). The boundary element method and the finite element method can investigate the crack propagation in turbine blades (Citarella, Cricrì, Lepore, & Perrella, 2014; Citarella, Giannella, Vivo, Mazzeo, & Mechanics, 2016; Fossati, Colombo, Manes, & Giglio, 2011). A common problem in modeling cracks in the blade is mismatching due to the critical mesh gradient (Peng, Atroshchenko, Kerfriden, & Bordas, 2017). Therefore, the type of element representing the discontinuities, like crack's singularity, can have a significant role in fracture analysis (Liu et al., 2020). Several types of the element have been applied for accurate crack modeling and stress region singularities in turbine blades, such as hexahedral element (Fawaz, 1998; Nikishkov & Atluri, 1987; Shivakumar, Tan, & Newman Jr, 1988), tetrahedral element (Okada, Kawai, & Araki, 2008; Okada, Kawai, Tokuda, & Fukui, 2013; Okada, Koya, Kawai, Li, & Osakabe, 2016; Rajaram, Socrate, & Parks, 2000) and quadratic element (Barsoum, 1976). In this context, some meshing method has been proposed in which there were mesh refining loop free from the singular element (Han, Wang, Yin, & Wang, 2015). Moreover, the gradual transition method (Koshima & Okada, 2015), which is not dependent on mesh for representing the explicit form of crack proposed for mesh generation, including less fine meshes and coarse meshes (Branco, Antunes, Ricardo, Costa, & Design, 2012; Branco, Rodrigues, Antunes, Materials, & Structures, 2008) and also 3D qualified mesh analysis like XFEM (Sukumar, Dolbow, & Moës, 2015) and GFEM (O'Hara, Duarte, & Eason, 2016). Recently, some crack mesh methods called "template mesh" (O'Hara et al., 2016) and automatic mesh generation methods called "rapid development method" (A. O. J. I. j. o. s. Ayhan &

structures, 2011; Bremberg & Dhondt, 2008) have been proposed in which meshing at crack tip vicinity are stable and not very sensitive to refining for achieving accuracy (Garcia-Manrique, Camas, Gonzalez-Herrera, Materials, & Structures, 2017). However, regardless of the applied mesh type for crack front or crack tip vicinity, highly meshing strategies should be considered to evaluate fracture parameters, e.g., SIF. The weight functions (A.-j. Chen & Zeng, 2006; Jones & Rothwell, 2001; Kaiping & Chun-tu, 2004; Seifi, 2015), the singular integral equations (Noda & Xu, 2008; Tweed, Das, & Rooke, 1972; Tweed & Rooke, 1973), the boundary collocation (Theo Fett, 2002; YH Wang, Tham, Lee, & Tsui, 2003), the boundary element (Maschke & Kuna, 1985; Mavrothanasis & Pavlou, 2007), the finite element (Branco & Antunes, 2008; Kotousov, Berto, Lazzarin, & Pegorin, 2012; Sanati et al., 2015; Tsang, Oyadiji, & Leung, 2007), and the combination methods (Belytschko & Black, 1999; T Fett & Bahr, 1999; Vigdergauz, 1996) are common methods used for predicting SIFs.

Accurate estimation of crack parameters such as length and depth can be obtained by applying the semi-elliptical crack. Several types of research have been made for the representation of semi-elliptical crack in surface plates (Jin & Wang, 2013; Mattheck, Morawietz, & Munz, 1983; Mattheck, Munz, & Stamm, 1983; X. Wang, 2003; Xiao, Wang, Tu, & Xuan, 2020) (Lin & Smith, 1998b), pressure vessel (Çetin & Yaman, 2020), high-density polyethylene (Wee, Chudnovsky, Choi, & Structures, 2020), and etc. For instance, Mattheck, C. et al. (Mattheck, Morawietz, et al., 1983; Mattheck, Munz, et al., 1983) evaluated the SIF for cracked plate stress gradients using semi-elliptical crack. The method was mainly based on weight functions in which the Petroski and Achenbach approach obtained the crack opening displacement. 3D analysis has later been applied for calculating T-stress in thick cracked plate that was compared with empirical test results (X. Wang, 2003). Also, the weight function for semi-elliptical cracks can be used to determine the SIF and T-stress in thickness plates (Jin & Wang, 2013). Regarding the above literature, most of the research concentrated on failure analysis based on modeling edge/through the induced crack in the gas turbine blade. In the present study, a new approach has been proposed to investigate the nearby real aero-elastical behavior of crack-induced gas turbine blades. In this context, the turbine's rotational speed and aerodynamic remarks

such as fluid solid interaction have been modeled according to operating conditions. Then, a semi-elliptical crack has been considered in the critical zone of the rotating blade to achieve high accuracy. Eventually, SIFs for various crack locations and aspect ratios have been evaluated. In the present research, both of the structure and the aerodynamic analysis were considered on Al Alloys, Steel and Titanium gas turbine blade considering mixed mode (I/II/III) loading condition. Not only variation of mechanical properties (i.e. Al Alloys, Steel and Titanium blade), but also mixed mode (I/II/III) loading condition and simultaneous CFD simulation can be considered as the main difference between this work to others. In materials and methods section, the main numerical strategy including FSI and material properties were considered. In the results and discussion section, both of the structure and the aerodynamic analysis were considered on Al Alloys, steel and Titanium gas turbine blade considering mixed mode (I/II/III) loading condition. Also, mixed mode (I/II/III) SIFs were obtained for various crack location and aspect ratio.

## Materials and Methods

Considering several implementations of the gas turbine in several industries, the fracture study of the gas turbine blade can have a significant role in operational efficiency. In Fig. 1, the gas turbine rotor and blade have been shown.
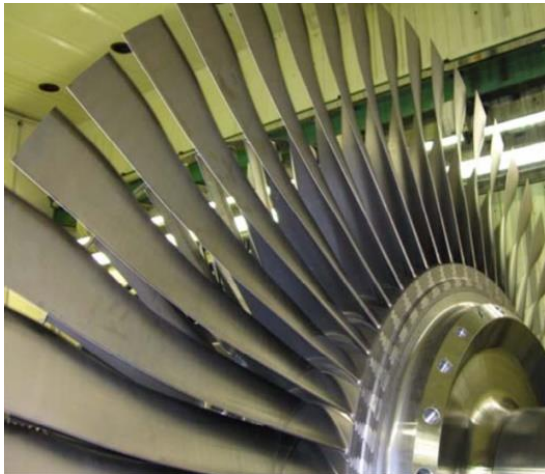


**Figure 1:** Gas turbine rotor and blade

### Semi-Elliptical Crack Specification

Based on experimental results, crack location is considered in various positions but mostly classified in the root, the middle, and the nearby tip of the blade. From overall considerations, the root location

of the crack can have a critical effect due to the maximum stressed concentration. Therefore, the present study attempts to identify the root location of the induced semi-elliptical crack. So, the geometry of the semi-elliptical crack configuration applied in the rotating blade (fig 2) can be described as the blade thickness ($t$), the width of the blade (b), the crack length ($c$), and the crack depth ($a$). Due to the mode mixity, the length of the crack can have any direction along the blade length.
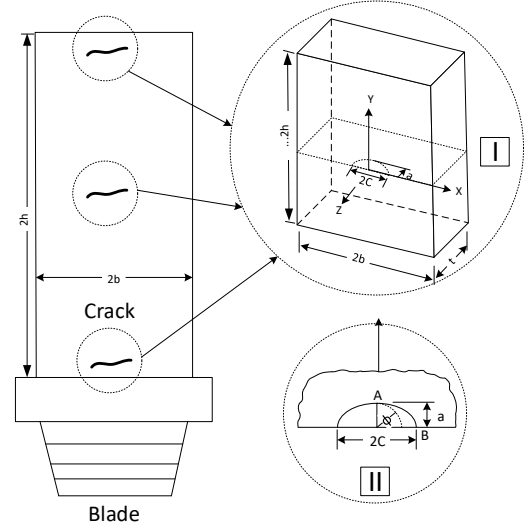


**Figure 2**: (I) and (II) denote the semi-elliptical crack specifications

In the rotating body, these factors are a function of load, crack length, crack depth, and geometry. These coefficients could be expressed as (Knott, 1973):

$$K_\text{I} = F_\text{I}\left(\frac{a}{c}, \frac{a}{t}, \frac{r_i}{r_o}\right) \times \sigma_0 \sqrt{\pi a}$$

$$K_\text{II} = F_\text{II}\left(\frac{a}{c}, \frac{a}{t}, \frac{r_i}{r_o}\right) \times \sigma_0 \sqrt{\pi a} \qquad (1)$$

$$K_\text{III} = F_\text{III}\left(\frac{a}{c}, \frac{a}{t}, \frac{r_i}{r_o}\right) \times \sigma_0 \sqrt{\pi a}$$

In which $F_\text{I}$, $F_\text{II,}$ and $F_\text{III}$ are geometrical coefficients in modes I, II, and III, respectively. $\sigma_0$ is the nominal stress and in the rotating bodies could be expressed as Eq. (2):

$$\sigma_0 = \frac{3+\upsilon}{8}\rho\omega^2\left(r_2^2 - r_1^2\right) \qquad (2)$$

In which, $\omega = 2\pi\left(rpm\right)/60$ .

## Numerical Strategy

The numerical sections were performed using both ANSYS Workbench software and MATLAB@ Coding. In this context, various circumferential semi-elliptical cracks with an aspect ratio of (a/c) 0.4 to 1 were modeled in ANSYS software. All cracks considered in this paper have a fixed length of 10 mm. Also, based on the aspect ratio of the considered cracks, the depth of cracks varied between 2 to 5 mm. Table 1 shows the typical geometrical configuration and material properties of the gas turbine blade and rotor used in this study.

**Table 1**: The geometrical configuration and material properties applied in numerical analysis

| Parameters | Definition | Value |
|---|---|---|
| $r_i$ | Inner radius of rotor | 10 cm |
| $r_o$ | Outer radius of rotor | 30 cm |
| $t$ | Thickness of blade | 2 cm |
| $2c$ | Length of semi-elliptical cracks | 10 mm |
| $a$ | Depth of semi-elliptical cracks | 2 to 5 mm |
| $E_{St}$ | Elastic modulus of steel blade | 200 GPa |
| $\upsilon_{St}$ | Poisson's ratio of steel blade | 0.3 |
| $\rho_{St}$ | Density of steel blade | 7850 kg/m$^3$ |
| $E_{Al}$ | Elastic modulus of aluminum blade | 71 GPa |
| $\upsilon_{AL}$ | Poisson's ratio of aluminum blade | 0.33 |
| $\rho_{AL}$ | Density of aluminum blade | 2770 kg/m$^3$ |
| $E_{Ti}$ | Elastic modulus of titanium blade | 96 GPa |
| $\upsilon_{Ti}$ | Poisson's ratio of titanium blade | 0.36 |
| $\rho_{Ti}$ | Density of titanium blade | 4620 kg/m$^3$ |

Fig. 3 shows the 3D model and the mesh pattern generated for the numerical solution of the gas turbine blade. Based on this figure, 20 noded solid brick elements with quadratic interpolation were used for numerical solution in ANSYS Workbench software.
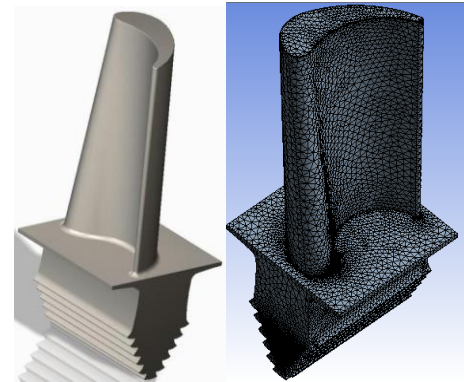


**Figure 3**: (a) and (b) represent the 3D model and the mesh pattern generated for gas turbine blade

Fig. 4 shows the crack face and the points on the crack face for various aspect ratios and generalized semi-elliptical configuration based on the dimensionless distance of *x/c*.
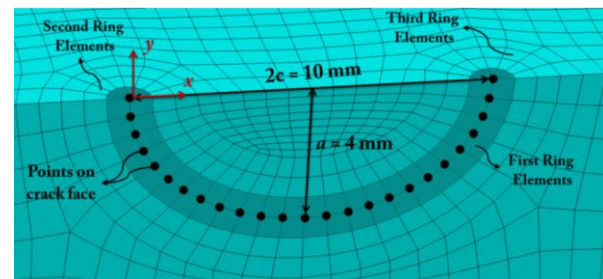


**Figure 4**: Crack face and corresponding points related to a semi-elliptical crack with aspect ratio of 0.8

As it was described, during a real operation, the crack can be located at the root, middle, and tip of the blade (Fig.5). Based on several types of research, the critical mode of stress concentration was figured out at the root of the blade.
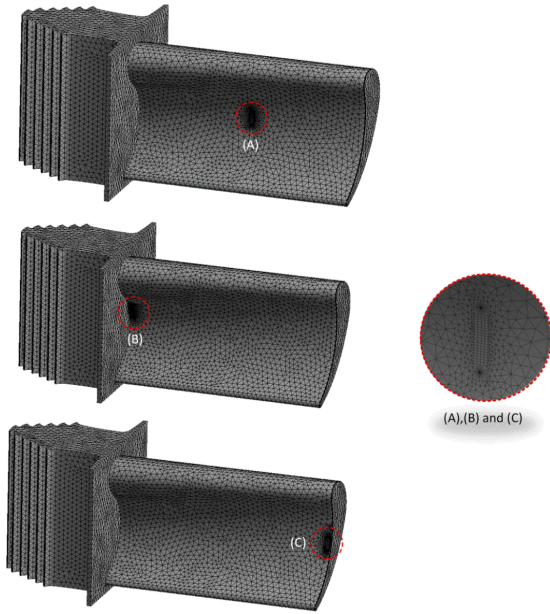
**Figure 5:** Crack location considered in the present research

In the numeric basis of crack tip singularity, enriched crack tip elements should be considered for obtaining SIFs. In this context, not only 2D asymptotic field of displacements can represent the crack tip (Benzley, 1974), but also the usual polynomial interpolation function was considered (A. Ayhan & Nied, 2002; A. O. Ayhan, 2000; A. O. J. I. J. o. F. Ayhan, 2007; A. O. J. I. j. o. s. Ayhan & structures, 2011). However, the enriched element displacements (i.e., u, v, and w) can take the form as follows (A. Ayhan & Nied, 2002; A. O. Ayhan, 2000).

$$u(\xi,\eta,\rho) = \sum_{j=1}^{r} N_j(\xi,\eta,\rho)u_j + Z_0(\xi,\eta,\rho)\{K_I(\Gamma)F_1(\xi,\eta,\rho)$$
$$+ K_{II}(\Gamma)G_1(\xi,\eta,\rho) + K_{III}(\Gamma)H_1(\xi,\eta,\rho)\}$$

$$v(\xi,\eta,\rho) = \sum_{j=1}^{r} N_j(\xi,\eta,\rho)v_j + Z_0(\xi,\eta,\rho)\{K_I(\Gamma)F_2(\xi,\eta,\rho)$$
$$+ K_{II}(\Gamma)G_2(\xi,\eta,\rho) + K_{III}(\Gamma)H_2(\xi,\eta,\rho)\} \quad (3)$$

$$w(\xi,\eta,\rho) = \sum_{j=1}^{r} N_j(\xi,\eta,\rho)w_j + Z_0(\xi,\eta,\rho)\{K_I(\Gamma)F_3(\xi,\eta,\rho)$$
$$+ K_{II}(\Gamma)G_3(\xi,\eta,\rho) + K_{III}(\Gamma)H_3(\xi,\eta,\rho)\}$$

In which $u_j$, $v_j$, $w_j$, and $N_j(\xi,\eta,\rho)$ represent the unknown nodal displacements and the element shape functions. Moreover, $K_I(\Gamma)$, $K_{II}(\Gamma)$, and $K_{III}(\Gamma)$ represent the mode I, II, and III SIF corresponding to interpolation functions $N_i(\Gamma)$. The stress intensity factors vary along the crack front as:

$$K_I(\Gamma) = \sum_{m=1}^{s} K_I^m N_m(\Gamma)$$

$$K_{II}(\Gamma) = \sum_{m=1}^{s} K_{II}^m N_m(\Gamma) \quad (4)$$

$$K_{III}(\Gamma) = \sum_{m=1}^{s} K_{III}^m N_m(\Gamma)$$

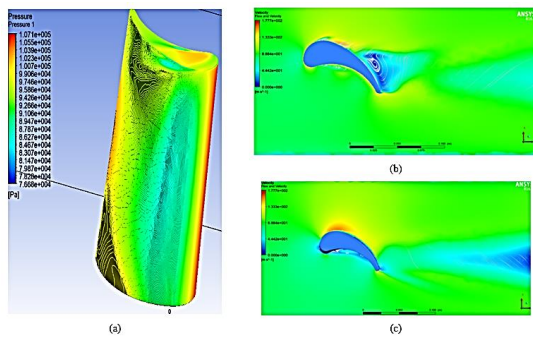For the present study, the mixed-mode fracture was investigated using 3D FEM.

## Flow Solid Interaction Modeling

To simulate the full wind turbine configuration and to investigate the rotor–tower interaction, a 3D model of the gas turbine blade in the tunnel was modeled and analyzed employing SOLID WORKS and ANSYS WORKBENCH (Version 16.1), respectively. Running a temperature was also considered 25 °C and airflow speed at 83.776 m/s (Bernstein & Allen, 1992). Simple mesh is considered for meshing the fluid with a growth rate of 1.10, edge sizing with 50 divisions, and fine element size. Fig. 6 shows the CFX Boundary conditions and mesh refining.



(a)



(b)
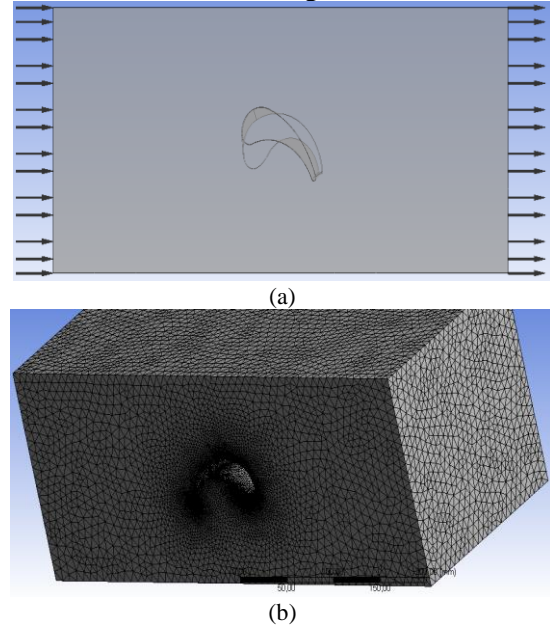
**Figure 6:** (a) CFX Boundary conditions (named by Inlet, Outlet, Wall and Blade) (b) CFX mesh refining for Flow and Blade domain

In the static structure setup, the pressure was applied on all external surfaces of the blade, and mechanical nodes were mapped to the CFD surface with an element size of 2.5 mm. Also, boundary conditions were considered as fixed support with no large deflection. CFD simulation was done at a speed of 83.776 m/s, and the results have been performed from different blade sections for pressure, flow, and velocity (Fig. 7).

The 3D finite element modeling of semi-elliptical cracks was considered using 20 noded solid brick elements with quadratic interpolation for crack modeling and 15 noded quarter-point singular wedge elements for the crack front. The total number of the element was 136135. Structure simulation was done at the speed of 83.776 m/s. Fig. 8 shows the total deformation and equivalent (Von-Mises) stress at 17 m/s in the blade.



**Figure 7:** (a) Minimum and maximum pressure applied on blade (b) and (c) represent as fluid flow and velocity in the top and middle surface of blade
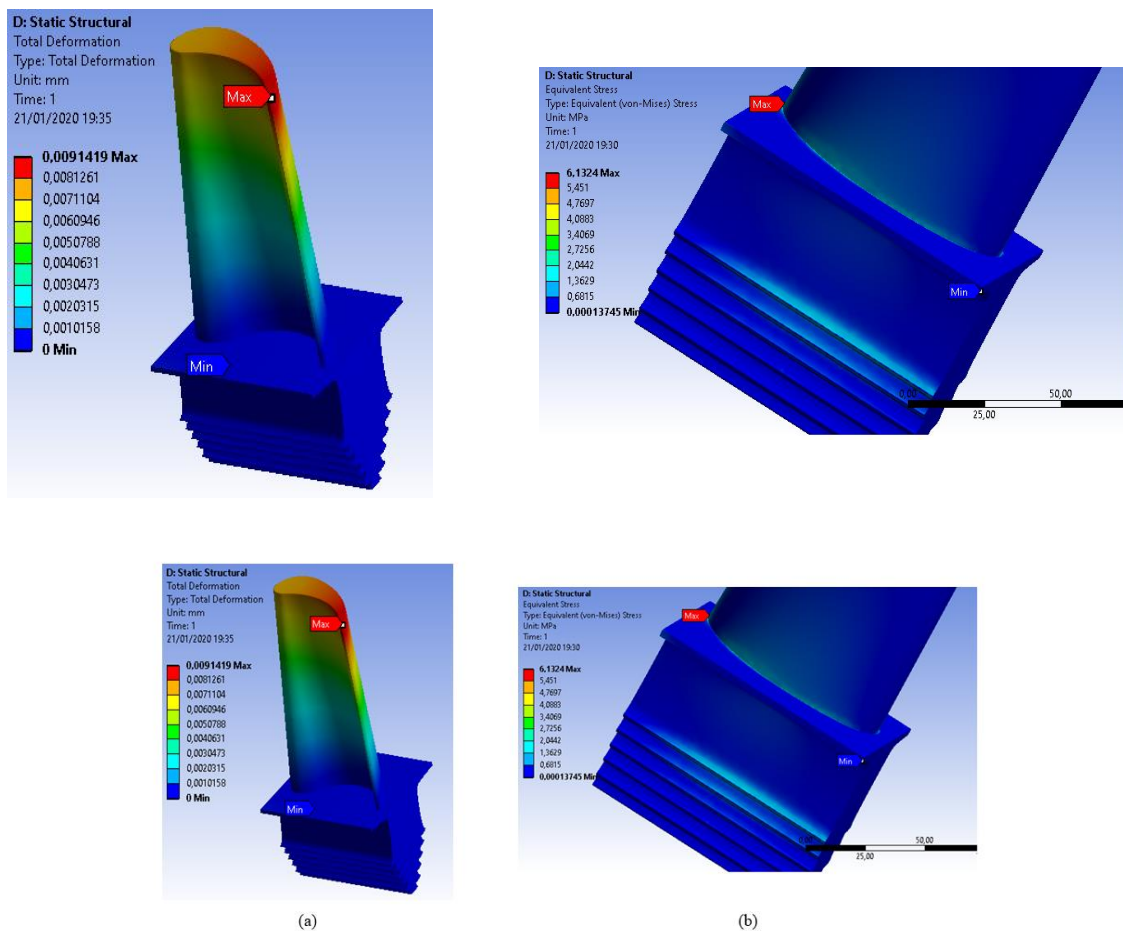


**Figure 8:** (a) Total deformation in blade (b) Equivalent (von-Mises) stress at 17 m/s in blade

## Results and Discussion

### Verification

In this section, the modeling and analysis procedure employed in this study are verified. In this regard, the results of Liu et al. (Liu et al., 2020) have been used. They could simulate the 3D crack propagation in turbine blades precisely. They also considered a turbine blade and calculated stress intensity factors by utilizing FRANC3D for a semi-elliptical crack in the mentioned blade. Fig. 9 shows the geometrical schematic of the considered semi-elliptical crack by Liu et al. (Liu et al., 2020) in the turbine blade.
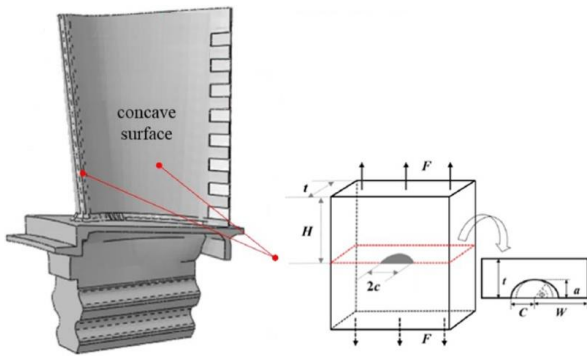
**Figure 9**: Geometrical schematic of the considered semi-elliptical crack by Liu et al. (Liu et al., 2020) in turbine blade

Table 2 shows the dimensions of the semi-elliptical crack and material properties employed by Liu et al. (Liu et al., 2020).

**Table 2**: The dimensions of the semi-elliptical crack and material properties employed by Liu et al. (Liu et al., 2020)

| W (mm) | H (mm) | T (mm) | a (mm) | c (mm) | E (MPa) | $\upsilon$ |
|---|---|---|---|---|---|---|
| 4 | 4 | 2 | 1 | 1 | 100000 | 0.3 |

For verification of the modeling and analysis procedure employed in this study, the mentioned turbine blade was modeled in ANSYS software. The results of SIF were compared with the results reported by Liu et al. Fig. 10 shows the comparison of results between this study and the results reported by Liu et al. Based on this figure, good compatibility could be shown between the results, which confirms the employed method in modeling and analysis procedure in this study.
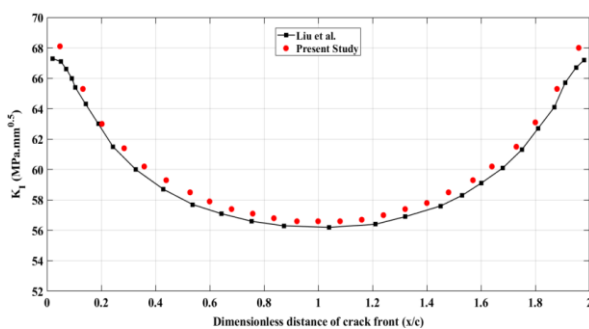


**Figure 10**: Comparison of results between presented study and reported results by Liu et al. (Liu et al., 2020)

**Numerical Calculation of Fracture Parameters**

In the present section, the effect of crack aspect ratio, rotational velocity, crack location, and mechanical properties of the blade have been studied on fracture parameters. Before presenting numerical results of fracture

parameters in blades, convergence studies to determine a sufficient number of elements to ensure from the accuracy of results should be done. In this regards, the maximum value of mode I stress intensity factor for steel blade with 2000 rpm rotational velocity with different aspect ratios for various number of elements has been studied. Results of convergence analysis are shown in Fig. 11. Based on this Figure, it is revealed that, after about 140000 elements, the numerical results have been converged. Therefore, the optimal number of elements to ensure from the accuracy of results in the numerical simulation is 140000 elements approximately.
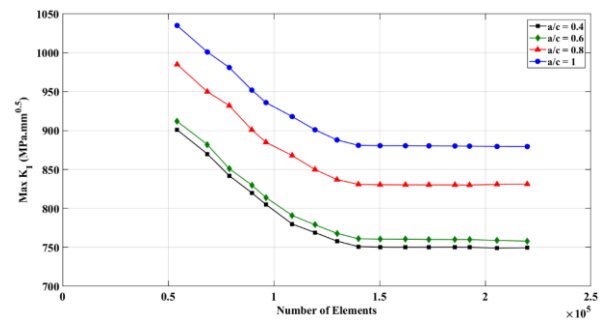


**Figure 11**: Convergence of maximum mode I stress intensity factor for steel blade with 2000 rpm rotational velocity with different aspect ratios

The static stress analysis and centrifugal stresses were investigated. Detailed view of crack tip for semi-elliptical cracks was illustrated with specific aspect ratio considering rotational velocity (Fig. 12).
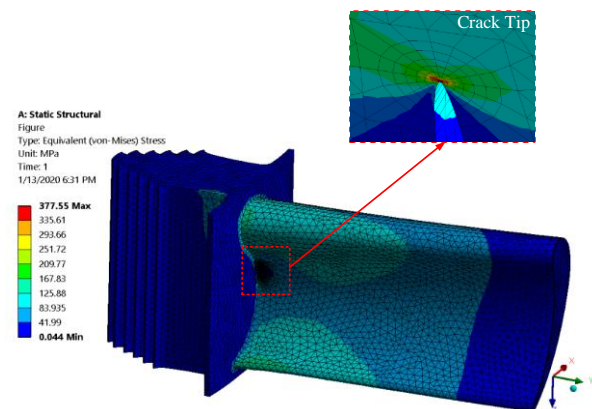


**Figure 12**: Detailed view of crack tip for semi-elliptical cracks with aspect ratio of 0.8 in steel blade with rotational velocity of 1000 rpm

Variations of SIFs versus front crack distance were considered to investigate the effect of crack aspect ratio on fracture parameters. In this regard, variations of mode I, II, and III SIF through crack front distance for steel blade with 2000 rotational velocity with different aspect ratios are presented in Fig. 13. Based on this figure, it is revealed that, for cracks with dimension ratios of 0.4 to 0.6, the maximum value of mode I SIF occurred in the depths point of the crack front. In contrast, for cracks with dimension ratios of 0.8 to 1, maximum values of mode I SIF occurred near free surfaces of the crack front. Therefore, by increasing the aspect ratios, the location of the critical point of mode I SIF on the crack front varied from the depths point to the free surfaces of the crack front. But, the critical point location of mode II and III SIFs on the crack front did not vary by the crack aspect ratio. The maximum values of mode II and III SIFs occurred in the depths point and free surfaces of the crack front, respectively. Also, by considering this figure, it is revealed that, in the location of $x/c$= 0.6 and 1.4, mode I SIF is independent of crack aspect ratio and, in the location of $x/c$= 0.9, mode III SIF is independent of crack dimension ratio.
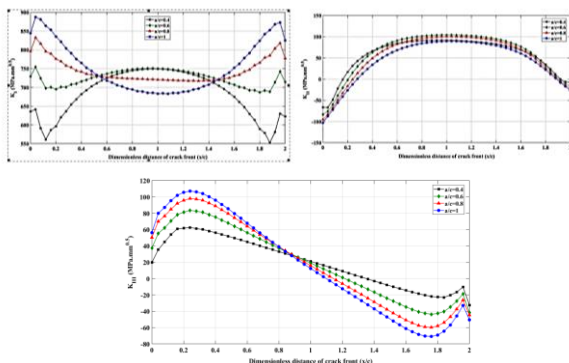


**Figure 13**: Variations of mode I/II/III SIF through crack front distance for steel blade with 2000 rotational velocity and specified aspect ratio

Moreover, the effect of the rotational velocity on fracture parameters was investigated based on SIF variations through a specified aspect ratio. In this regard, variations of mode I, II, and III SIFs through the crack front for steel blade with an aspect ratio of 0.8 with different rotational velocities are presented in Fig. 14. Based on this figure, it is revealed that the mode I, II, and III SIFs are increased by an increase in the rotational velocity of blades. By exploring these figures, it is found that by increasing rotational velocity from 500 rpm to 2000 rpm, the maximum increase in mode I, II, and III SIFs are 1560, 1330,

and 1407 percent, respectively. Therefore, mode I SIF has a higher sensitivity to the increase of rotational velocity of blades. Also, by considering this figure, it is revealed that, near the location of $x/c$= 0.25 and 1.9, mode II SIF is independent of rotational velocity and, near the location of $x/c$= 1.1, mode III SIF is independent of rotational velocity of blades.
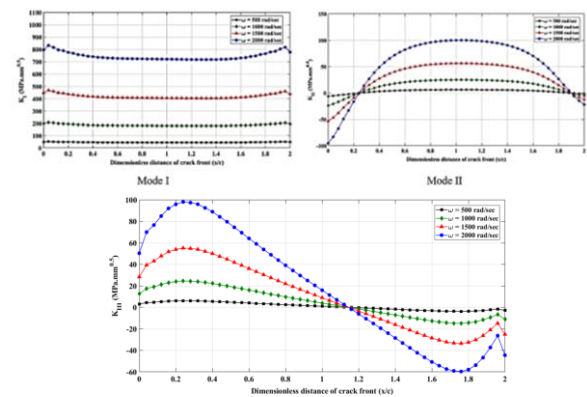


**Figure 14**: Variations of mode I/II/III SIF through crack front with aspect ratio of 0.8 in steel blade with different rotational velocity

The effects of mechanical properties of gas turbine blades are also investigated. In this regard, Steel, Aluminum, and Titanium blades are considered, and fracture parameters for these materials are compared. Variations of mode I, II, and III SIFs through the crack front distance for different blade material based on 2000 rpm rotational velocity and dimension ratio of 1 are illustrated in Fig. 15. According to this figure, it is quite clear that increasing the blade density causes a significant increase in centrifugal stresses and, thereby, stress intensity factors. Thus, the Aluminum blade is the most resistant to crack propagation.

Moreover, it is found that, near the location of $x/c$= 0.25 and 1.9, mode II SIF is independent of mechanical properties, and near the location of $x/c$= 1.1, mode III SIF is independent of mechanical properties of blades. Therefore, near the location of $x/c$= 0.25 and 1.9 in crack front, mode II SIF is independent of rotational velocity and blades' mechanical properties. Also, near the location of $x/c$= 1.1 in crack front, mode III SIF is independent of rotational velocity and blades' mechanical properties.
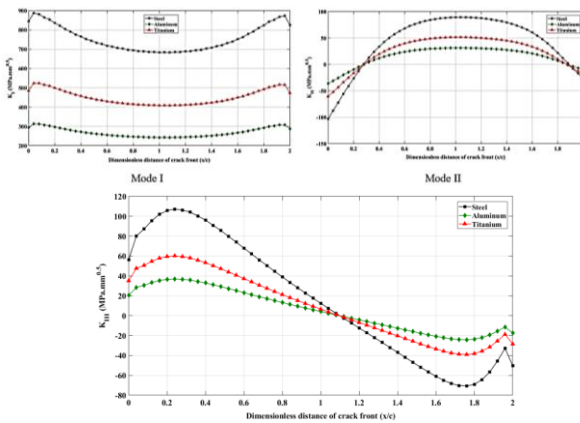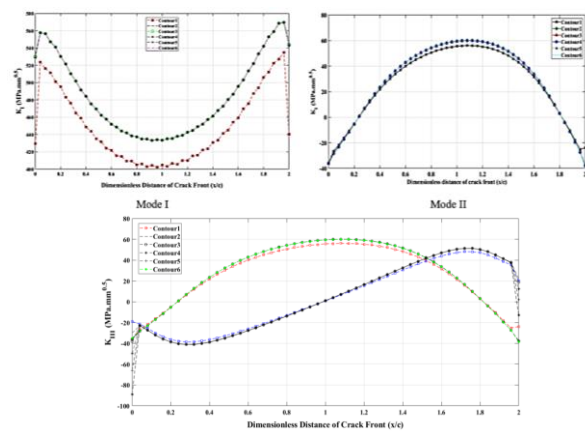
**Figure 15**: Variations of mode I/II/III SIF through crack front distance for different blade's material considering 2000 rpm rotational velocity and specified aspect ratio

Effects of the location of a crack in fracture parameters are investigated in Fig. 16. In this regard, variations of mode I, II, and III SIFs through the crack front for cracks with dimensions ratio of 0.6 in steel blade with a rotational velocity of 2000 rpm and different locations are presented in Fig. 16. Based on this figure, it is clear that cracks on the root are the most critical in gas turbine blades.
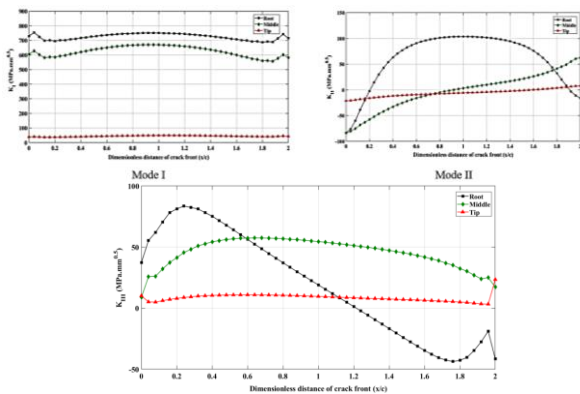


**Figure 16**: Variations of mode I/II/III SIF through crack front for semi-elliptical cracks with aspect ratio of 0.6 in steel blade with rotational velocity of 2000 rpm and different location

Fig. 17 shows the sufficient overviewing of contour effectiveness in the mode I, II, and III SIF by considering FSI evaluation. As it can be figured out from this figure, SIFs that were obtained on the basis of the 6th contour were more in accordance with non-aerodynamic. Quadratic nodal displacement and interpolation functions can have more accuracy in the 6th contour when the aerodynamic remark is considered.



**Figure 17**: Variations of mode I/II/III SIF through crack front for semi-elliptical cracks with aspect ratio of 0.6 in steel blade with rotational velocity of 2000 rpm and different location

## Conclusions

In this study, a numerical approach has been proposed to investigate the fracture behavior of gas turbine blades represented by the stress intensity factor. In this context, the turbine's rotational speed and aerodynamic remarks such as fluid-solid interaction have been modeled according to operating conditions. Then, semi-elliptical crack under mixed-mode loading (I/II/III) condition has been considered in the critical zone of the rotating blade to achieve the effect of crack aspect ratio, rotational velocity, crack location, and mechanical properties. Results showed that by increasing the aspect ratios, the location of the critical point of mode I SIF can be varied from depths point to free surfaces of the crack front. Whereas the location of the critical point of mode II and III SIFs on the crack front does not differ from the crack dimension ratio. Also, the results indicated that cracks on the root in gas turbine blades are the most critical, and the Al Alloys blade shows a profitable resistance in crack propagation. Moreover, as the crack domain is near the location of x/c= 0.25 and 1.9 of crack front, the mode II SIF will be independent of rotational velocity and the blades' mechanical properties. Similarly, for the location of *x/c*= 1.1 in crack front, the mode III SIF is independent of rotational velocity and blades' mechanical properties.

## References

1- Ayhan, A., & Nied, H. J. I. J. f. N. M. i. E. (2002). Stress intensity factors for three-dimensional surface cracks using enriched finite elements. *54*(6), 899-921.

2- Ayhan, A. O. (2000). Finite element analysis of nonlinear deformation mechanisms in semiconductor packages.

3- Ayhan, A. O. J. I. J. o. F. (2007). Mixed mode stress intensity factors for deflected and inclined corner cracks in finite-thickness plates. *29*(2), 305-317.

4- Ayhan, A. O. J. I. j. o. s., & structures. (2011). Three-dimensional fracture analysis using tetrahedral enriched elements and fully unstructured mesh. *48*(3-4), 492-505.

5- Barsoum, R. S. J. I. j. f. n. m. i. e. (1976). On the use of isoparametric finite elements in linear fracture mechanics. *10*(1), 25-37.

6- Belytschko, T., & Black, T. (1999). Elastic crack growth in finite elements with minimal remeshing. *International journal for numerical methods in engineering, 45*(5), 601-620.

7- Benzley, S. J. I. J. f. N. M. i. E. (1974). Representation of singularities with isoparametric finite elements. *8*(3), 537-545.

8- Bernstein, H. L., & Allen, J. M. (1992). Analysis of cracked gas turbine blades.

9- Boyce, M. P. (2011). *Gas turbine engineering handbook*: Elsevier.

10- Branco, R., & Antunes, F. (2008). Finite element modelling and analysis of crack shape evolution in mode-I fatigue Middle Cracked Tension specimens. *Engineering fracture mechanics, 75*(10), 3020-3037.

11- Branco, R., Antunes, F., Ricardo, L., Costa, J. J. F. E. i. A., & Design. (2012). Extent of surface regions near corner points of notched cracked bodies subjected to mode-I loading. *50*, 147-160.

12- Branco, R., Rodrigues, D., Antunes, F. J. F., Materials, F. o. E., & Structures. (2008). Influence of through-thickness crack shape on plasticity induced crack closure. *31*(2), 209-220.

13- Bremberg, D., & Dhondt, G. J. E. F. M. (2008). Automatic crack-insertion for arbitrary crack growth. *75*(3-4), 404-416.

14- Çetin, M., & Yaman, K. J. D. S. J. (2020). Location, Size and Orientation Effect of Semi-elliptical Surface Crack on the Fracture of a Type-3 Composite Pressure Vessel using J-integral Method. *70*(1), 23-34.

15- Chen, A.-j., & Zeng, W.-j. (2006). Weight function for stress intensity factors in rotating thick-walled cylinder. *Applied Mathematics and Mechanics, 27*, 29-35.

16- Chen, L.-j., & Xie, L.-y. (2005). Prediction of high-temperature low-cycle fatigue life of aeroengine's turbine blades at low-pressure stage. *JOURNAL-NORTHEASTERN UNIVERSITY NATURAL SCIENCE, 26*(7), 673.

17- Citarella, R., Cricrì, G., Lepore, M., & Perrella, M. J. A. i. E. S. (2014). Thermo-mechanical crack propagation in aircraft engine vane by coupled FEM–DBEM approach. *67*, 57-69.

18- Citarella, R., Giannella, V., Vivo, E., Mazzeo, M. J. T., & Mechanics, A. F. (2016). FEM-DBEM approach for crack propagation in a low pressure aeroengine turbine vane segment. *86*, 143-152.

19- arrahi, G., Tirehdast, M., Abad, E. M. K., Parsa, S., & Motakefpoor, M. (2011). Failure analysis of a gas turbine compressor. *Engineering Failure Analysis, 18*(1), 474-484.

20- Fawaz, S. J. E. F. M. (1998). Application of the virtual crack closure technique to calculate stress intensity factors for through cracks with an elliptical crack front. *59*(3), 327-342.

21- Fett, T. (2002). Stress intensity factors and T-stress for single and double-edge-cracked circular disks under mixed boundary conditions. *Engineering fracture mechanics, 69*(1), 69-83.

22- Fett, T., & Bahr, H. (1999). Mode I stress intensity factors and weight functions for short plates under different boundary conditions. *Engineering fracture mechanics, 62*(6), 593-606.

23- Fossati, M., Colombo, D., Manes, A., & Giglio, M. J. E. f. m. (2011). Numerical modelling of crack growth profiles in integral skin-stringer panels. *78*(7), 1341-1352

24- Funazaki, K., Tarukawa, Y., Kudo, T., Matsuno, S., Imai, R., & Yamawaki, S. (2001). *Heat Transfer Characteristics of an Integrated Cooling Configuration for Ultra-High Temperature Turbine Blades: Experimental and Numerical Investigations.* Paper presented at the ASME Turbo Expo 2001: Power for Land, Sea, and Air.

25- arcia-Manrique, J., Camas, D., Gonzalez-Herrera, A. J. F., Materials, F. o. E., & Structures. (2017). Study of the stress intensity factor analysis through thickness: methodological aspects. *40*(8), 1295-1308

26- Garzon, V. E., & Darmofal, D. L. (2003). Impact of geometric variability on axial compressor performance. *J. Turbomach., 125*(4), 692-703.

27- Ghatak, A., & Robi, P. (2016). Modification of Larson–Miller parameter technique for predicting creep life of materials. *Transactions of the Indian Institute of Metals, 69*(2), 579-583.

28- Guo, X., Zheng, W., Xiao, C., Li, L., Antonov, S., Zheng, Y., & Feng, Q. (2019). Evaluation of microstructural degradation in a failed gas turbine blade due to overheating. *Engineering Failure Analysis, 103*, 308-318.

29- Han, Q., Wang, Y., Yin, Y., & Wang, D. J. E. F. M. (2015). Determination of stress intensity factor for mode I fatigue crack based on finite element analysis. *138*, 118-126.

30- Hirakawa, K., Toyama, K., & Kubota, M. J. I. j. o. f. (1998). The analysis and prevention of failure in railway axles. *20*(2), 135-144.

31- Hou, J., Wicks, B. J., & Antoniou, R. A. (2002). An investigation of fatigue failures of turbine blades in a gas turbine engine by mechanical analysis. *Engineering Failure Analysis, 9*(2), 201-211.

32- Jin, Z., & Wang, X. (2013). Weight functions for the determination of stress intensity factor and T-stress for semi-elliptical cracks in finite thickness plate. *Fatigue & Fracture of Engineering Materials & Structures, 36*(10), 1051-1066.

33- Jones, I., & Rothwell, G. (2001). Reference stress intensity factors with application to weight functions for internal circumferential cracks in cylinders. *Engineering Fracture Mechanics, 68*(4), 435-454.

34- Kai-ping, M., & Chun-tu, L. (2004). Semi-weight function method on computation of stress intensity factors in dissimilar materials. *Applied Mathematics and Mechanics, 25*(11), 1241-1248.

35- Kersey, R., Staroselsky, A., Dudzinski, D., & Genest, M. J. I. j. o. f. (2013). Thermomechanical fatigue crack growth from laser drilled holes in single crystal nickel based superalloy. *55*, 183-193.

36- Kirthan, L., Hegde, R., Suresh, B., & Kumar, R. G. J. P. M. S. (2014). Computational analysis of fatigue crack growth based on stress intensity factor approach in axial flow compressor blades. *5*, 387-397.

37- Knott, J. F. (1973). *Fundamentals of fracture mechanics*: Gruppo Italiano Frattura.

38- Koshima, T., & Okada, H. J. E. F. M. (2015). Three-dimensional J-integral evaluation for finite strain elastic–

plastic solid using the quadratic tetrahedral finite element and automatic meshing methodology. *135*, 34-63.

39- Kotousov, A., Berto, F., Lazzarin, P., & Pegorin, F. (2012). Three dimensional finite element mixed fracture mode under anti-plane loading of a crack. *Theoretical and Applied Fracture Mechanics, 62*, 26-33.

40- Kumar, A., Keane, A., Nair, P., & Shahpar, S. (2006). *Robust design of compressor blades against manufacturing variations.* Paper presented at the ASME 2006 International Design Engineering Technical Conferences and Computers and Information in Engineering Conference.

41- Kumar, A., Nair, P., Keane, A., & Shahpar, S. (2005). *Probabilistic performance analysis of eroded compressor blades.* Paper presented at the ASME 2005 power conference.

42- Kumari, S., Satyanarayana, D., & Srinivas, M. J. E. f. a. (2014). Failure analysis of gas turbine rotor blades. *45*, 234-244.

43- Lakshminarasimha, A., Boyce, M., & Meher-Homji, C. (1994). Modeling and analysis of gas turbine performance deterioration.

44- Lange, A., Vogeler, K., Schrapp, H., & Clemen, C. (2009). *Introduction of a parameter based compressor blade model for considering measured geometry uncertainties in numerical simulation.* Paper presented at the ASME Turbo Expo 2009: Power for Land, Sea, and Air.

45- Li, Y.-G. (2010). Gas turbine performance and health status estimation using adaptive gas path analysis. *Journal of engineering for gas turbines and power, 132*(4).

46- Lin, X., & Smith, R. (1998a). Fatigue growth prediction of internal surface cracks in pressure vessels.

47- Lin, X., & Smith, R. (1998b). Fatigue growth prediction of internal surface cracks in pressure vessels. *Journal of pressure vessel technology, 120*(1), 17-23.

48- Liu, H., Yang, X., Li, S., & Shi, D. J. I. J. o. M. S. (2020). A numerical approach to simulate 3D crack propagation in turbine blades. *171*, 105408.

49- Maschke, H.-G., & Kuna, M. (1985). A review of boundary and finite element methods in fracture mechanics. *Theoretical and Applied Fracture Mechanics, 4*(3), 181-189.

50- Mattheck, C., Morawietz, P., & Munz, D. (1983). Stress intensity factor at the surface and at the deepest point of a semi-elliptical surface crack in plates under stress gradients. *International Journal of Fracture, 23*(3), 201-212.

51- Mattheck, C., Munz, D., & Stamm, H. (1983). Stress intensity factor for semi-elliptical surface cracks loaded by stress gradients. *Engineering fracture mechanics, 18*(3), 633-641. doi:https://doi.org/10.1016/0013-7944(83)90056-5

52- Mavrothanasis, F., & Pavlou, D. (2007). Mode-I stress intensity factor derivation by a suitable Green's function. *Engineering analysis with boundary elements, 31*(2), 184-190.

53- Montoya, J. (1966). Coupled bending and torsional vibrations in a twisted rotating blade. *The Brown Boveri Review, 53*(3), 216-230.

54- Morini, M., Pinelli, M., Spina, P. R., & Venturini, M. (2011). Numerical analysis of the effects of nonuniform surface roughness on compressor stage performance. *Journal of engineering for gas turbines and power, 133*(7).

55- Mouna, A., Boukortt, H., Meliani, M. H., Muthana, B. D., Suleiman, R. K., Sorour, A. A., . . . Azari, Z. (2019). CORROSION EFFECT, CONSTRAINT AND PATH ORIENTATION ESTIMATED IN CRACKED GAS TURBINE BLADE. *Engineering Failure Analysis*, 104345.

56- Nikishkov, G., & Atluri, S. J. I. j. f. n. m. i. e. (1987). Calculation of fracture mechanics parameters for an arbitrary three-dimensional crack, by the 'equivalent domain integral'method. *24*(9), 1801-1821.

57- Noda, N.-A., & Xu, C. (2008). Controlling parameter of the stress intensity factors for a planar interfacial crack in three-dimensional bimaterials. *International Journal of Solids and Structures, 45*(3), 1017-1031.

58- Nowell, D., Dini, D., & Hills, D. J. E. f. m. (2006). Recent developments in the understanding of fretting fatigue. *73*(2), 207-222.

59- O'Hara, P., Duarte, C. A., & Eason, T. J. E. F. M. (2016). A two-scale generalized finite element method for interaction and coalescence of multiple crack surfaces. *163*, 274-302.

60- Okada, H., Kawai, H., & Araki, K. J. E. F. M. (2008). A virtual crack closure-integral method (VCCM) to compute the energy release rates and stress intensity factors based on quadratic tetrahedral finite elements. *75*(15), 4466-4485.

61- Okada, H., Kawai, H., Tokuda, T., & Fukui, Y. J. I. j. o. f. (2013). Fully automated mixed mode crack propagation analyses based on tetrahedral finite element and VCCM (virtual crack closure-integral method). *50*, 33-39.

62- Okada, H., Koya, H., Kawai, H., Li, Y., & Osakabe, K. J. E. F. M. (2016). Computations of stress intensity factors for semi-elliptical cracks with high aspect ratios by using the tetrahedral finite element (fully automated parametric study). *158*, 144-166.

63- Peng, X., Atroshchenko, E., Kerfriden, P., & Bordas, S. P. A. J. I. J. o. F. (2017). Linear elastic fracture simulation directly from CAD: 2D NURBS-based implementation and role of tip enrichment. *204*(1), 55-78.

64- Poursaeidi, E., Aieneravaie, M., & Mohammadi, M. (2008). Failure analysis of a second stage blade in a gas turbine engine. *Engineering Failure Analysis, 15*(8), 1111-1129.

65- Poursaeidi, E., & Salavatian, M. J. E. F. A. (2009). Fatigue crack growth simulation in a generator fan blade. *16*(3), 888-898.

66- Rajaram, H., Socrate, S., & Parks, D. J. E. F. M. (2000). Application of domain integral methods using tetrahedral elements to the determination of stress intensity factors. *66*(5), 455-482.

67- Sanati, H., Amini, A., Reshadi, F., Soltani, N., Faraji, G., & Zalnezhad, E. (2015). The stress intensity factors (SIFs) of cracked half-plane specimen in contact with semi-circular object. *Theoretical and Applied Fracture Mechanics, 75*, 104-112.

68- Sarraf, C., Nouri, H., Ravelet, F., & Bakir, F. (2011). Experimental study of blade thickness effects on the overall and local performances of a controlled vortex designed axial-flow fan. *Experimental Thermal and Fluid Science, 35*(4), 684-693.

69- Seifi, R. (2015). Stress intensity factors for internal surface cracks in autofrettaged functionally graded thick cylinders using weight function method. *Theoretical and Applied Fracture Mechanics, 75*, 113-123.

70- Shivakumar, K., Tan, P., & Newman Jr, J. (1988). A virtual crack-closure technique for calculating stress intensity factors for cracked three dimensional bodies.

71- Shojaeifard, M., Sajedin, A., & Khalkhali, A. J. M. M. E. (2019). Effectiveness of Blade Thickness Distribution on the Turbocharger Turbine Aerostatic Performance. *19*(11), 2667-2677.

72- Suder, K. L., Chima, R. V., Strazisar, A. J., & Roberts, W. B. (1995). The effect of adding roughness and thickness to a transonic axial compressor rotor.

73- Sukumar, N., Dolbow, J., & Moës, N. J. I. J. o. F. (2015). Extended finite element method in computational fracture mechanics: a retrospective examination. *196*(1-2), 189-206.

74- Tao, C., Zhong, P., & Li, R. (2000). Failure analysis and prevention for rotor in aero-engine. *National Defence Industry Press, China*, 102-163.

75- Tsang, D., Oyadiji, S., & Leung, A. (2007). Two-dimensional fractal-like finite element method for thermoelastic crack analysis. *International Journal of Solids and Structures, 44*(24), 7862-7876.

76- Tweed, J., Das, S., & Rooke, D. (1972). The stress intensity factors of a radial crack in a finite elastic disc. *International Journal of Engineering Science, 10*(3), 323-335.

77- Tweed, J., & Rooke, D. (1973). The stress intensity factor of an edge crack in a finite elastic disc. *International Journal of Engineering Science, 11*(1), 65-73.

78- Vigdergauz, S. (1996). An effective method for computing the elastic field in a finite cracked disk. *Engineering fracture mechanics, 53*(4), 545-556.

79- Viswanathan, R., & Dolbec, A. (1987). Life assessment technology for combustion turbine blades.

80- Wang, X. (2003). Elastic T-stress solutions for semi-elliptical surface cracks in finite thickness plates. *Engineering fracture mechanics, 70*(6), 731-756. doi:https://doi.org/10.1016/S0013-7944(02)00081-4

81- Wang, Y., & Susmel, L. (2016). The Modified Manson–Coffin Curve Method to estimate fatigue lifetime under complex constant and variable amplitude multiaxial fatigue loading. *International Journal of Fatigue, 83*, 135-149.

82- Wang, Y., Tham, L., Lee, P., & Tsui, Y. (2003). A boundary collocation method for cracked plates. *Computers & structures, 81*(28), 2621-2630.

83- Wee, J.-W., Chudnovsky, A., Choi, B.-H. J. I. J. o. S., & Structures. (2020). Discontinuous slow crack growth modeling of semi-elliptical surface crack in high density polyethylene using crack layer theory. *185*, 65-77.

84- Witek, L. J. E. F. A. (2015). Simulation of crack growth in the compressor blade subjected to resonant vibration using hybrid method. *49*, 57-66.

85- Witek, L. J. F. o. A. S. (2012). Numerical simulation of fatigue fracture of the turbine disc. *2012*(4), 114-122.

86- Xi, N., Zhong, P., Huang, H., Yan, H., & Tao, C. J. E. f. a. (2000). Failure investigation of blade and disk in first stage compressor. *7*(6), 385-392.

87- Xiao, J., Wang, G., Tu, S., & Xuan, F. J. E. F. M. (2020). Engineering estimation method of unified constraint parameters for semi-elliptical surface cracks in plates. 106935.

88- Yang, S., Hui, B., & Guo-tai, F. (2011). *Investigation and application of high accuracy schemes in numerical simulation of turbine flow field.* Paper presented at the 2011 International Conference on Mechatronic Science, Electric Engineering and Computer (MEC).

89- Yasmina, A., Bacha, N., & Semmar, D. (2008). Probabilistic model for pitting corrosion and fatigue life estimation of turbine blades [J]. *Integritet I Vek Konstrukcija, 8*(1), 3-12.

90- Ying, Y., Cao, Y., Li, S., Li, J., & Guo, J. (2016). Study on gas turbine engine fault diagnostic approach with a hybrid of gray relation theory and gas-path analysis. *Advances in Mechanical Engineering, 8*(1), 1687814015627769.

91- Yu, Z.-Y., Zhu, S.-P., Liu, Q., & Liu, Y. (2017). A new energy-critical plane damage parameter for multiaxial fatigue life prediction of turbine blades. *Materials, 10*(5), 513.

92- Zhou, D., Wei, T., Huang, D., Li, Y., & Zhang, H. (2020). A gas path fault diagnostic model of gas turbines based on changes of blade profiles. *Engineering Failure Analysis*, 104377.